Available online at www.sciencedirect.com
ScienceDirect
Biochimica et Biophysica Acta 1768 (2007) 3012–3019
Biochimica et Biophysica Acta
BBA
www.elsevier.com/locate/bbamem

Proteorhodopsin: Characterisation of 2D crystals by electron microscopy and solid state NMR

Sarika Shastri [a], Janet Vonck [b], Nicole Pfleger [a], Winfried Haase [b], Werner Kuehlbrandt [b], Clemens Glaubitz [a,*]

[a] *Institute of Biophysical Chemistry, Centre for Biomolecular Magnetic Resonance, J.W. Goethe University, Max von Laue Str. 9, D-60438 Frankfurt am Main, Germany*
[b] *Max Planck Institute of Biophysics, Max von Laue Str. 3, D-60438 Frankfurt am Main, Germany*

Received 30 July 2007; received in revised form 29 September 2007; accepted 2 October 2007
Available online 9 October 2007

Abstract

Proteorhodopsin (PR) a recent addition to retinal type 1 protein family, is a bacterial homologue of archaeal bacteriorhodopsin. It was found to high abundance in γ-proteobacteria in the photic zone of the oceans and has been shown to act as a photoactive proton pump. It is therefore involved in the utilisation of light energy for energy production within the cell. Based on data from biodiversity screens, hundreds of variants were discovered worldwide, which are spectrally tuned to the available light at different locations in the sea. Here, we present a characterisation of 2D crystals of the green variant of proteorhodopsin by electron microscopy and solid state NMR. 2D crystal formation with hexagonal protein packing was observed under a very wide range of conditions indicating that PR might be also closely packed under native conditions. A low-resolution 2D projection map reveals a ring-shaped oligomeric assembly of PR. The protein state was analysed by ^{15}N MAS NMR on lysine, tryptophan and methionine labelled samples. The chemical shift of the protonated Schiff base was almost identical to non-crystalline preparations. All residues could be cross-polarised in non-frozen samples. Lee–Goldberg cross-polarisation has been used to probe protein backbone mobility.

Keywords: Solid state NMR; 2D crystallography; Membrane protein; Reconstitution; Proteorhodopsin

1. Introduction

It has been estimated that the world's oceans contain 10^{28} bacteria expressing the recently discovered light-driven proton pump proteorhodopsin [1] which makes an important contribution to the conversion of chemical energy from light. Discovery of PR in these marine γ-proteobacteria extends the representation of type 1 rhodopsin family to the domain of bacteria [2]. Hundreds of PR variants have been found which are spectrally tuned to the light availability of the habitat [3–6]. They can be broadly classified into two subgroups based on their absorption maxima: green PR (~520 nm) and blue PR (~490 nm). They share about 80% sequence identity making them potential candidates for detailed studies to understand the origin of spectral tuning.

Despite 26% sequence identity, PR is different from archaeal bacteriorhodopsin (bR) as it shows a higher sequence homology to sensory rhodopsin and is found in bacteria suggesting a different evolutionary origin [7]. PR has no ionisable extracellular groups for a fast release of protons to the extracellular medium. The pK_a of the primary proton acceptor in PR is five pH units higher compared to bR (PR: p$K_{a,D97}$ ~ 7.2, bR: p$K_{a,\ D85}$ ~ 2.5) [8]. The primary proton acceptor D85, the proton donor D96, the Schiff base linkage K216 and the counter ions of the Schiff base R82 and D212 in bR correspond to D97, E108, K231, R94 and D227 in PR, respectively. A homology model of PR is shown in Fig. 1.

In PR as in bR, the absorption of light alters the retinal conformation from all-*trans* to 13-*cis* initiating a photo cycle which culminates in the transfer of protons from the inside to the outside of the cell. A photo cycle involving proton transport

Abbreviations: (bR), bacteriorhodopsin; (CP), cross-polarisation; (CSA), chemical shift anisotropy; (CMC), critical micelle concentration; (DDM), *n*-dodecyl β-D-maltoside; (DP), direct polarisation; (HETCOR), heteronuclear correlation; (OG), octyl-beta-D-glucopyranoside; (PR), proteorhodopsin

* Corresponding author. Tel.: +49 69 798 29927; fax: +49 69 798 29929.
E-mail address: glaubitz@em.uni-frankfurt.de (C. Glaubitz).

0005-2736/$ - see front matter © 2007 Elsevier B.V. All rights reserved.
doi:10.1016/j.bbamem.2007.10.001

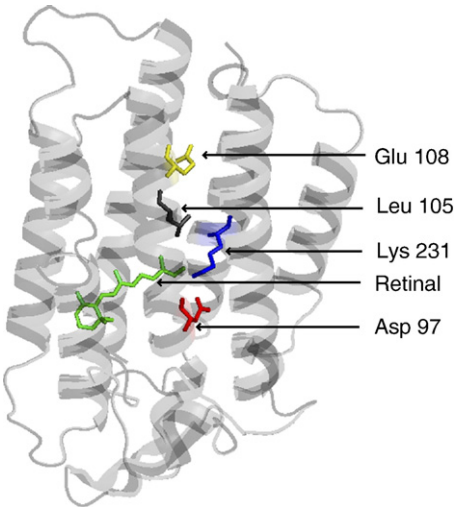

Fig. 1. Homology model of PR based on bR (1c3w). Chromophore retinal and essential residues E108 (primary proton donor), D97 (primary proton acceptor), K231 (Schiff base) and L105 (responsible for colour tuning) are highlighted.

is initiated at alkaline pH (pH > p$K_{a,D97}$) [9] but experiments by Friedrich et al. have also shown an inversion at pH < p$K_{a,D97}$ [8]. This suggests that PR may also have a regulatory function. The potential importance of PR for energy conversion has been illustrated by "light-powering" *Escherichia coli* cells expressing PR when cellular respiration is inhibited [1] and by light-stimulated growth of PR containing marine Flavobacteria [10]. The photo cycle of PR has been studied spectroscopically in some detail [8,11–13] but structural data are not yet available.

Recently, we have reported the first solid state NMR study on retinal and Schiff base in green proteorhodopsin reconstituted in lipid bilayers [14]. Our data did show that the chromophore exists mainly in the all-*trans* configuration in the proteorhodopsin ground state. The optical absorption maximum (~520 nm) together with retinal and Schiff base chemical shifts indicates a strong interaction network between chromophore and opsin. Both observations are supported by FTIR studies [15,16]. One bottleneck encountered when working with large membrane proteins like PR, is the high protein concentration needed while maintaining a membrane like environment. We have previously reported functional reconstitution of an ABC multidrug transporter for solid state NMR [17]. Higher concentrations have been achieved for example by preparing 3D crystals of the membrane protein DGK [18] or by precipitating the transmembrane enzyme DsbB [19]. However, the best way to ensure a membrane environment at high protein concentration is 2D crystallisation, as demonstrated for the β-barrel outer-membrane porin OmpG [20]. We have therefore prepared isotope labelled green proteorhodopsin as 2D crystals and report a first characterisation of these samples by electron microscopy and solid state NMR.

2. Materials and methods

2.1. Materials

All-*trans*-retinal was obtained from Sigma-Aldrich, unlabelled amino acids and nucleotide bases for the defined medium from AppliChem, all labelled amino acids from Eurisotop, LB medium from Roth, 1, 2-dioleolyl-*sn*-glycero-3-phosphocholine (DOPC) from Avanti Polar Lipids. *N*-dodecyl β-D-maltoside (DDM) was obtained from AppliChem, *n*-octyl β-D-glucopyranoside (OG) from GLYCON Biochem GmbH, Triton X-100 from AppliChem and Ni-NTA agarose from Qiagen.

2.2. Expression and purification of PR

Expression of wild type PR was essentially done as described elsewhere [8,14]. Depending on the intended use, the cells were grown in LB medium (for crystallisation screens) or in defined medium [21] (for specific labelling) or minimal medium for uniform labelling. 50 μg/ml kanamycin was used and cells were collected when an OD_{578} of 0.8 was reached. After spinning down, cells were resuspended in fresh medium. In case of labelled preparations, fresh medium containing labelled amino acids was introduced at this stage. After 15 min of incubation, 1 mM IPTG and 0.7 mM of all-*trans* retinal dissolved in ethanol were added. Overexpression was achieved by a further incubation at 37 °C for 3–4 h and was visually observed by a pink colour change of the cells. The cells were harvested by centrifugation and cells were broken using a Constant System cell disrupter at 1.5–2 kbar. The recovered membrane pellet was solubilised with 1.5% DDM overnight. Detergent solubilised PR (supernatant) was obtained by ultra-centrifugation and was incubated with Ni-NTA beads for approximately 1 h. After thorough washing, the protein was finally eluted in 0.2% Triton X-100. Purity of preparation was checked on SDS PAGE, UV–Vis spectroscopy and gel filtration.

2.3. 2D crystal preparation

DOPC in chloroform was dried in a stream of nitrogen for about 30 min followed by vacuum drying. Lipid was solubilised in 2% OG dissolved in equilibration buffer (20 mM MES, 300 mM NaCl, pH 6.0) at a concentration of 5 mg/ml and sonicated until clear. PR was reconstituted at a very low lipid to protein ratio of ~0.25 (w/w). Typical crystalline preparations involved slow detergent removal by dialysis with the aid of dialysis tubes (14 kDa cut-off) against excess of dialysis buffer (50 mM Tricin, 100 mM NaCl, 10 mM $MgCl_2$, 3 mM NaN_3, 5 mM DTT, pH 8.5, 7.5% MPD). The dialysis buffer was changed every day and the crystalline samples were obtained after 7 days. These samples were then used either for electron microscopy or NMR measurements.

2.4. Electron microscopy

2D crystalline samples in 5 μl aliquots were applied to freshly glow-discharged carbon coated copper grids (400 mesh) and allowed to incubate at room temperature for 2 min. The grids were placed upside down on 2% uranyl acetate (pH 4.5) and held for 30 s to remove excess of sample. The grid was finally air dried. Grids were examined in a Philips CM120 electron microscope with an accelerating voltage of 120 kV at a magnification of 45,000× or 60,000×. Additionally freeze-fracture replicas produced in the freeze-fracture unit BAF400T (Bal-TEC Inc., Principality of Liechtenstein) were analysed in an EM208S electron microscope (FEI Company). Images were collected on a 2K × 2K slow-scan CCD camera (Gatan Inc.). Crystal images were processed using the MRC program package [22].

2.5. Sample preparation for solid state NMR

After dialysis, 2D crystals were ultra-centrifuged at 45,000 rpm for 30 min at 4 °C. The pellet was subjected to series of washes and ultra-centrifugation steps to remove the excess detergent. Finally the pellet was transferred to a 4 mm MAS rotor and sealed by a thin silicon disc [23]. Depending on preparation and expression yield, the rotor contained 5–15 mg of sample. All NMR experiments were carried out on non-frozen samples at 280 K.

2.6. NMR measurement

^{31}P and ^{15}N MAS NMR experiments were carried out on Bruker Avance 400 and 600 NMR spectrometers, which were equipped with 4 mm MAS DVT probeheads. Standard parameters were used for cross- and direct polarisation experiments (50 ms acquisition time with 90 kHz ^{1}H spinal-64 decoupling [24],

4 μs ^{1}H 90° pulse, 3–5 μs×90° pulses, 1–1.5 ms cross-polarisation contact times with a ramped proton spin-lock field, 1–2 s recycle delay times). Larmor frequencies for ^{1}H, ^{31}P, and ^{15}N were 600.13, 242.88, and 60.8 MHz at the Avance 600 and 400.13, 161.92, and 40.5 MHz at the Avance 400, respectively. Sample rotation rates used for MAS were between 3 and 14 kHz. Details are given in the figure legends.

^{15}N chemical shift — ^{15}N–^{1}H dipolar correlation spectra were acquired using Lee–Goldburg cross-polarisation (LG-CP) [25,26]. The CP contact time was incremented by 30 μs 128 times resulting in a t_1 evolution time of 3.84 ms. Experiments were carried out at 12 kHz sample spinning. The ^{15}N spin-lock field was adjusted to the first order sideband condition. Only cosine modulated data were collected and a real Fourier transformation was applied to the indirect dimension. To remove the dominant zero frequency peak caused by the signal increase with increasing contact time, an exponential baseline correction was applied prior to Fourier transformation. ^{15}N/^{1}H two dimensional heteronuclear spectroscopy (HETCOR) [27] was performed using frequency switched Lee–Goldburg decoupling at an effective proton decoupling field of 85 kHz during the evolution period and two pulse phase modulation proton decoupling at 64 kHz during the acquisition period. 2 k scans in the ω_2 dimension and 64 rows in the ω_1 dimension were acquired using time-proportional phase increments. The scaling factor for the ω_1 dimension was determined to be 0.57. A spinning rate of 14 kHz was used. Both LG-CP and HETCOR experiments were carried out using a Bruker Avance 400.

^{15}N and ^{31}P spectra were referenced externally to $(^{15}NH_4)_2SO_4$ at 27 ppm and 10% phosphoric acid at 0 ppm, respectively. Data were processed using Topspin 2.0 (Bruker, Karlsruhe, Germany).

3. Results and discussion

3.1. Characterisation of PR 2D crystals by electron microscopy

Our 2D crystallisation screen was initially motivated by the similarities between bR and PR, and the fact that bR is arranged in 2D arrays within the *Halobacterium salinarium* membrane [28]. However, nothing is known about the arrangement of PR protobacterial membranes. The first goal was therefore to find suitable 2D crystallisation conditions. High quality 2D crystals would provide structural data of PR and at the same time could also be used for detailed mechanistic studies by solid state NMR as natural 2D crystals of bR (purple membrane) did yield very well resolved spectra [29]. Major benefits of 2D crystals are high sample concentration and homogeneity. Furthermore, crystal packing would reduce internal molecular motions which might interfere with coherent averaging by magic angle sample spinning.

3.1.1. 2D crystallisation screen

In order to find the best crystallisation conditions, we have systematically varied the following parameters: pH (4–11), temperature (4 °C–50 °C), protein–lipid ratio (0.10–0.25 w/w, monovalent (KCl, NaCl, LiCl; 100 mM–1 M) and divalent salts ($MnCl_2$, $NiCl_2$, $CoCl_2$, $MgCl_2$, $BaCl_2$ and $CaCl_2$; 100 mM–1 M), protein concentration (100 μg/ml–5 mg/ml) and duration of dialysis (5 days to 4 weeks). We have tested a variety of lipids, such as POPC, POPG, DMPC, DOPC, DOPE, *E. coli* lipids, SoyPC and Archeal lipids. A range of non-ionic, zwitterionic, cationic and anionic detergents was screened. All together, over 750 conditions were tested and checked for sample homogeneity by density gradient centrifugation and for formation of 2D crystals by electron microscopy. This systematic screen resulted finally in more than 700 successful crystallisation conditions with comparable sample quality but low diffraction. This means that the success rate of obtaining at least low diffracting 2D crystals is relatively high. Results of the EM analysis are discussed further below.

It is interesting to analyse the effect of variations of different reconstitution parameters on the formation of crystalline PR arrays within the membrane. The use of appropriate detergents for membrane protein stabilisation and crystallisation plays a crucial role and has been discussed extensively [30]. Initially, we screened various kinds of detergents with respect to protein stability and ease of removal by dialysis. It was found that protein was stable in Triton X-100, OG and DDM as observed by UV/VIS absorption spectroscopy. Considering the effect of the CMC on the duration of the dialysis, the detergent screen was further expanded to the use of different combinations of detergents for protein elution and lipid solubilisation. The best combination was achieved with PR eluted in non-ionic Triton X-100 (CMC of 0.25–0.3 mM) and lipid solubilisation in OG (CMC of 20–25 mM) [31]. A dialysis time of typically one week with regular buffer changes was used. PR formed 2D crystals in all tested lipids but not in DMPC, possibly due to its short chains. A low lipid to protein ratio of about 0.20 (w/w) was essential for the formation of homogenous 2D crystalline samples. Increasing the amount of lipids to more than ~0.25 (w/w) led to formation of isolated crystalline patches that apparently prevented further growth of these areas. Unfortunately, highly ordered 2D crystalline sheets or vesicles which would be ideal for 2D crystallography were not obtained under any conditions tested.

Interestingly, the pH of the reconstitution buffer played a crucial role for the quality of the diffraction pattern. Reconstitution under acidic condition (pH 6) led to diffused, low order diffraction spots, compared to those obtained under physiological condition (pH 7). At alkaline pH (up to 11), the quality of crystals improved slightly (Fig. 2b). The pH of sea water is around 7.2–8.5 [32], which means that most PR molecules in a marine bacterium under native conditions are pumping protons from inside the cell to the outside. As the pK_a of the proton acceptor is ~7.2 of the proton acceptor [33], PR is either inactive or transports protons in opposite direction at acidic pH, which could lead to a heterogeneous mixture of molecules in different conformational states, leading to the diffused diffraction spots.

3.1.2. EM analysis

The best 2D crystals were obtained using synthetic lipids (DOPC) at pH 10 using an initial lipid to protein ratio of ~0.20 (w/w). The size of the crystalline vesicles was in the order of 0.5 μm (Fig. 2a) and the best diffraction pattern is shown in Fig. 2b. The crystalline arrangement of PR becomes especially clear using freeze-fracture electron microscopy (Fig. 2c). We have calculated a projection map from a negatively stained sample (Fig. 2d). Because the negative stain does not penetrate in the membrane, the projection map only depicts parts of the protein sticking out of the membrane. As can be seen in the Fourier transform (Fig. 2b), the protein has a hexagonal packing as in the case of bR. However, the resolution of 37 Å does not allow distinguishing between 3-fold or 6-fold symmetry. A

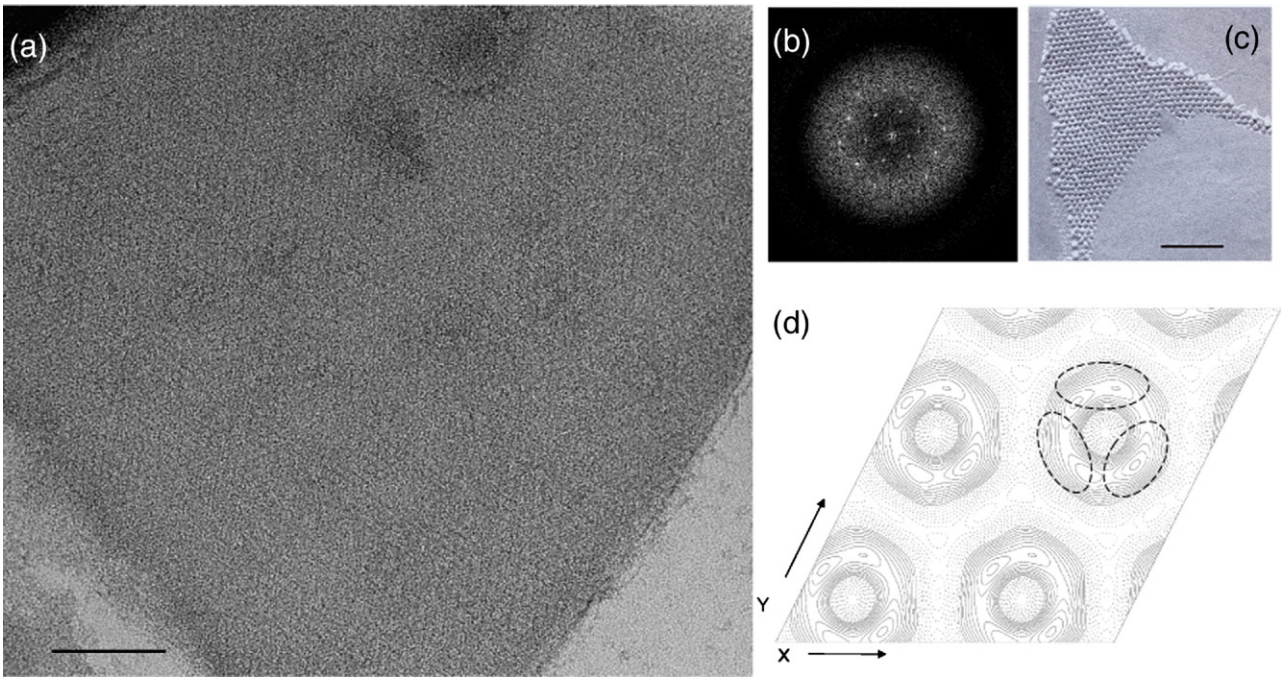

Fig. 2. Best 2D crystals of PR were obtained in DOPC at pH 10 (a). Fourier transformation of (a) shows two orders of diffraction spots (b). Freeze-fracture EM image depicts the 2D crystalline arrangement of our PR samples (c). A projection map in negative stain has been calculated (d) at a resolution of 37 Å. The parts of the protein protruding out of the membrane correspond to high density regions (solid contours) in the map. The unit cell dimensions are 87 Å × 87 Å. Two by two unit cells are shown. PR oligomerises into a ring-shaped assembly. The dashed lines depict a possible trimeric arrangement but a higher oligomeric state would be possible as well. Scale bars in (a) and (c) are 100 nm.

comparison with the well resolved structure of bR could indicate a trimeric arrangement [34] but a higher oligomer would be possible as well: The calculated size of the unit cell of 87 Å × 87 Å is too large for an individual PR molecule and supports this assumption. The protomers assemble into a ring-like structure with an average diameter of 42 Å. Liang et al. have recently described the role of electrostatic interactions in guiding the assembly of PR towards 2D and 3D arrays [35]. Their main emphasis has been on matching the charge density between PR and the membrane as the driving force for the formation of arrays for which they have used specifically charged lipids. Their conclusions about an oligomeric arrangement of PR within a hexagonal lattice, is consistent with our electron microscopy data. The formation of any ordered protein arrangements within the membrane could be driven by entropy, protein–protein or protein–lipid interactions. In case of PR, the same low-resolution 2D crystals were obtained under a wide range of conditions, which would hint towards dominating protein–protein interactions. It could also indicate, that PR might form protein patches in the native membrane.

3.2. Characterisation of PR 2D crystals by solid state NMR

For a first solid state NMR analysis, we have selected the same crystallisation conditions as used for the EM analysis described above, but at pH 8.5, which is closer to native conditions. The EM data for pH 8.5 and pH 10 did not show any differences at the resolution currently available.

3.2.1. ^{31}P MAS NMR: lipids in 2D crystals

Lipid protein interactions are essential for successful 2D crystallisation and for protein activity. We have therefore acquired ^{31}P MAS NMR spectra in order to characterise DOPC, the lipid used for crystallisation. The experiments were carried out at 280 K which is above the DOPC main phase transition temperature. Fig. 3a shows direct polarised ^{31}P spectra under proton decoupling at low spinning speed (3 kHz). Two major resonances are found at 3.6 ppm and −0.6 ppm. While the less shielded resonance is rather narrow and disappears under cross-polarisation (Fig. 3b), the peak at −0.6 ppm shows significant line-broadening (2.5 ppm) and is surrounded by spinning sidebands indicating a large chemical shift anisotropy. A comparison with a spectrum of DOPC bilayers at the same temperature and spinning speed shows comparable isotropic and anisotropic chemical shifts but reduced line-broadening (0.1 ppm) (Fig. 3c). The spinning sidebands in Fig. 3 correspond to an axially symmetric CSA tensor typical for fluid lipid bilayers. The rotational diffusion of lipids is not restricted despite the very small lipid to protein ratio in the 2D crystalline preparation. The increased line width in Fig. 3b could be caused by chemical exchange between protein-bound and non-bound lipids or altered lipid dynamics within the 2D crystal. The narrow lipid signals in Fig. 3a found at around 3.6 ppm do not show any significant anisotropy. These could be co-purified *E. coli* lipids or lipids in residual amounts of small unilamellar vesicles. Whether DOPC forms a bound belt around PR or whether other bound lipids have been co-purified together with PR and contribute to

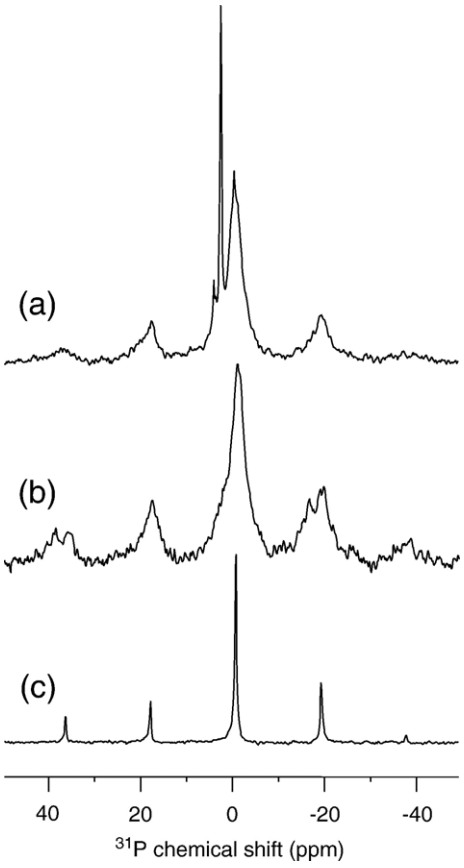

Fig. 3. ^{31}P direct polarised MAS spectrum (3 kHz spinning) of PR 2D crystals prepared in DOPC (a). The main species at −0.6 ppm shows a large CSA (CSA=33 ppm, η=0.1), while a minor population at 3.6 ppm is rather narrow and disappears under cross-polarisation (b). It could arise from other lipids co-purified with PR. For comparison, DOPC lipid bilayers are shown in (c) which show a similar axial symmetric CSA tensor (CSA=33 ppm, η=0) but reduced line width. Spectra were acquired with 40 k scans at 162 MHz for ^{31}P. The temperature was adjusted to 280 K to ensure a fully fluid lipid bilayer.

the ^{31}P signal cannot be decided at this point but is subject to further studies.

3.2.2. ^{15}N MAS NMR on ^{15}N-ζ-Lys labelled PR

In order to verify correct folding and functionality of PR in 2D crystalline form, we have prepared ^{15}N-ζ-Lys labelled samples. Lysine is the most conserved residue within the retinal binding pocket of proteins from the rhodopsin family. In PR, the chromophore retinal is covalently linked via a Schiff base to Lys-231. The ^{15}N chemical shift of this Schiff base is highly responsive to its protonation state [36] and an accurate reporter of photo cycle intermediates [37]. It has been studied extensively for photoisomerisation of retinal proteins [38]. The spectrum in Fig. 4a reveals a chemical shift of 185 ppm for the protonated Schiff base and 35.6 ppm for the other lysine side chains. The Schiff base chemical shift is almost identical to that in non-crystalline, reconstituted samples which are fully functional as reported previously [14]. In dark adapted bR, the PSB of the all-*trans* retinal resonates at 171 ppm and shows a λ_{max} at 568 nm which is different from PR (185 ppm and 520 nm). While the correlation between chemical shift and λ_{max} in bR agrees relatively well with PSB retinal model compounds [39], it deviates significantly for PR indicating very strong chromophore–opsin interactions [14,39]. It is important to note, that Schiff base, backbone amides and lysine side chains cross-polarise in non-frozen 2D crystalline samples while low temperatures (230 K) had to be used for the non-crystalline, reconstituted samples [14]. The line width has improved as well from 4.5 ppm to 0.5 ppm for the lysine side chains as a result of 2D crystallisation.

3.2.3. ^{15}N MAS NMR on a,ε-^{15}N-Trp labelled PR

Based on the observation that lysine side chains seem to be well ordered and able to cross-polarise in non-frozen samples, we have also tried to probe the 10 tryptophans found in PR. Based on homology models, residues 34, 74, 83, 159, 167, 197, and 239 are predicted to be located in the trans-membranous helical region while 58, 98, and 149 are probably found in loops or close to the membrane interface. Although not all 10 tryptophans can be resolved in 1D ^{15}N MAS NMR spectra, a number of well separated resonances with an average line width of 0.8 ppm from both backbone (115–129 ppm) and side chain (129–140 ppm) regions can be seen (Fig. 4b). This indicates a highly ordered backbone and side chain arrangement within 2D crystalline PR samples. The chemical shift range for backbone

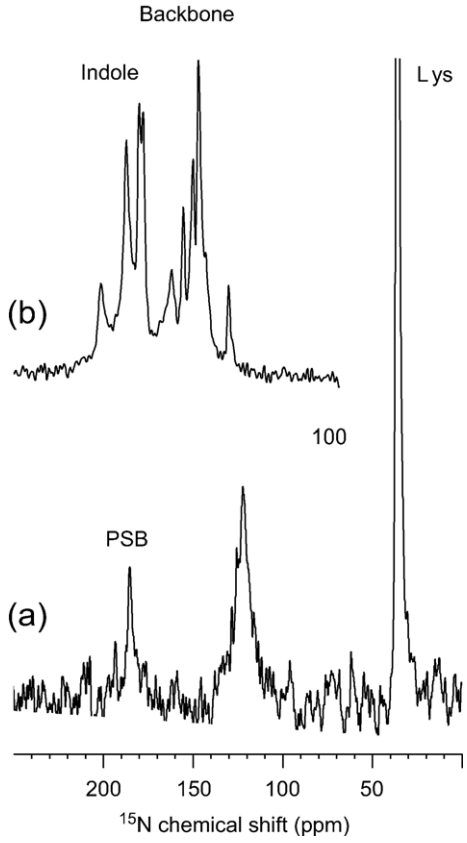

Fig. 4. ^{15}N-CP-MAS spectrum of ^{15}N-z-Lys 2D crystalline PR shows the protonated Schiff base (PSB) at 185 ppm (600 MHz, 11 kHz sample spinning, 30 k scans, 280 K) (a). The ^{15}N α-ε-Trp PR spectrum shows efficient cross-polarisation and good resolution of tryptophan side chain and backbone resonances in the non-frozen state (^{15}N at 40.5 MHz, 11 kHz sample spinning, 50 k scans, 280 K) (b).

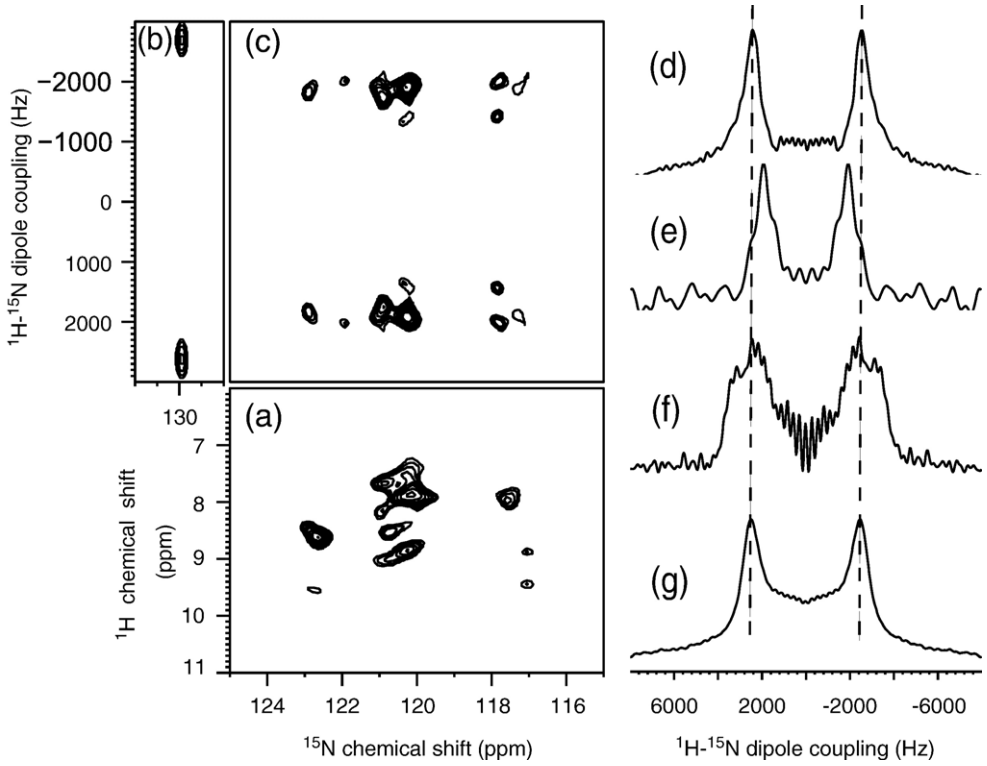

Fig. 5. ^{15}N–^{1}H HETCOR experiment of ^{15}N-Met PR reveals major intensities around 120 ppm but also at 123 and 117.5 ppm (a). The 2D ^{15}N–^{1}H LG-CP spectrum of ^{15}N-acetyl-leucine shows a rigid-limit dipolar splitting of 4.7 kHz (b), while the ^{15}N-Met resonances in PR show reduced dipolar splitting with an average value of 3.7 kHz indicating helix mobility despite 2D crystalline arrangement (c). A slice through the ^{15}N-acetyl-leucine spectrum at 130 ppm is shown in (d) and compared with ^{15}N-Met PR at 120 ppm in (e). The LG-CP spectrum of U–^{15}N PR (slice taken at 120 ppm) (f) deviates significantly from (e) indicating motions in PR caused by nonuniaxially motional averaging. Upon lowering the temperature to 220 K, the spectrum approaches a line shape expected for the rigid-limit case (d). All spectra were acquired at a 40.5 MHz for ^{15}N and 280 K except (e) where the temperature was adjusted to 220 K.

and side chain resonances is comparable to those reported for bovine rhodopsin [40]. A comparison of the observed chemical shifts for the backbone resonances with chemical shift data bases reveal, that the resonances are within the acceptable α-helical region [41]. Studies on bR have shown, that substitutions of tryptophan residues influence protein–retinal interactions [42]. Sequence alignment reveals that the Trp-197 is highly conserved in green PR, blue PR and bR, making a functional role likely although this needs further investigation.

3.2.4. ^{15}N MAS NMR on ^{15}N-Met labelled PR

In contrast to tryptophan, 9 out of 10 methionines (77, 79, 134, 140, 146, 162, 189, 190, 210) are buried inside the transmembranous region and only Met-189 is located at the interface. Compared to bR, these resonances did show a similar line width of 0.7 ppm but a smaller chemical shift dispersion of (6 ppm vs. 11 ppm [29]). We have therefore carried out ^{15}N–^{1}H HETCOR experiments (Fig. 5a). Most peaks are found around 120 ppm but cross-peak intensities are also seen at 123 ppm and 117.5 ppm.

Our data show, that highly ordered protein samples in 2D crystalline form in a non-frozen state provide well resolved spectra even of side chain resonances. Cross-polarisation at 280 K is possible, which indicates restricted protein dynamics. To probe this further, we have attempted to measure helix mobility by ^{15}N–^{1}H dipolar couplings using Lee–Goldberg cross-polarisation [43]. The experiment has been carried out first on crystalline ^{15}N-acetyl-leucine, where a rigid-limit, scaled dipolar splitting of 4.7 kHz is found (Fig. 5b). In PR, at 280 K, all ^{15}N–^{1}H methionine dipolar couplings are smaller with variations from residue to residue (in average 3.7 kHz). This corresponds to an order parameter of 0.8. A comparison between 1D slices through the spectra of ^{15}N-acetyl-leucine and ^{15}N-Met labelled PR is shown in Fig. 5d and e. The reduced splitting observed for methionine could partially be explained by the involvement in strong hydrogen bonds within the PR α-helices, but must contain some motional averaging due to small-angle wobbling of these individual residues, liberation of the peptide plane, or general fluctuations of the helices around their axis. To obtain a more global view, the same experiment was carried out on uniformly ^{15}N labelled proteorhodopsin. The spectrum obtained at 280 K (Fig. 5f) deviates clearly from the rigid-limit case shown in Fig. 5d but also from the selectively labelled sample in Fig. 5e. The dependence of Lee–Goldberg cross-polarisation line shapes on molecular motions had been discussed by Hong et al. [43]. Uniaxially motional averaging would just reduce the observed dipolar splitting while non-uniaxially dipolar averaging causes alterations in the spectral line shape such as broadening and additional wings on both sites of the spectrum. The spectrum in Fig. 5e shows a reduction in splitting but not a significant change in line shape compared to the rigid-limit case, while Fig. 5f reveals a line shape expected

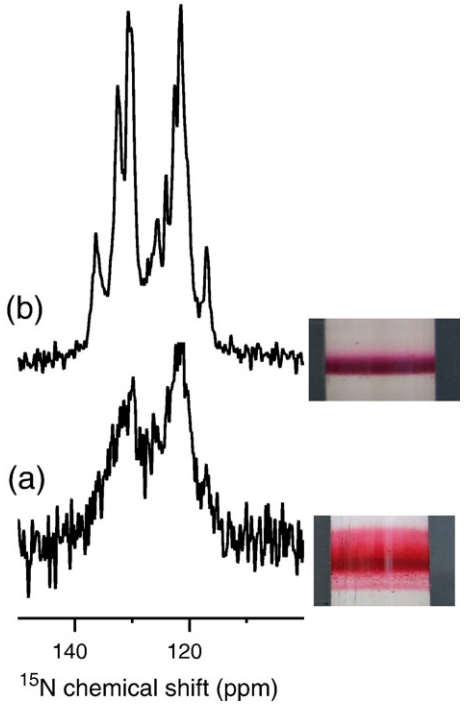

Fig. 6. ^{15}N-CP-MAS spectra of α-ε-^{15}N-tryptophan labelled PR without (a) and with additional washing steps after one week of dialysis (b). The observed poor resolution corresponds to a diffuse band when the sample is applied to a 60–90% density gradient under ultra-centrifugation. The band sharpens and spectra improve after sample washing.

for nonuniaxial dipolar averaging. Due to the overlap of 249 contributing N–H groups, a numerical analysis is not possible, but the spectrum shows, that PR undergoes anisotropic helix and loop fluctuations. A detailed characterisation requires further solid state NMR experiments in combination with different labelling schemes. By lowering the temperature to 220 K, most motions seem to be frozen out as the spectrum approaches the rigid-limit case. This is consistent with the observation that cross-polarisation at PR samples at this temperature yields a three-fold increase in signal-to-noise.

3.2.5. Practical aspects for solid state NMR on 2D crystals

When analysing various 2D crystalline preparations, we found that the quality of NMR spectra did not always correlate with data from electron microscopy. Two different samples of comparable quality as judged by freeze-fracture electron microscopy could differ with respect to spectral resolution. The problem was overcome by introducing additional washing steps after dialysis. Samples were repeatedly resuspended in buffer, pelleted and run over a 60–90% sucrose density gradient. Without additional washing, a diffuse band at 80% was sometimes observed which gave spectra of poor quality (Fig. 6a). With washing, the band sharpens, the sample cross-polarises better and shows enhanced resolution (Fig. 6b). One possible explanation for this observation could be the existence of residual amounts of detergents which might not influence diffraction properties of the sample at low temperature but may interfere with molecular motions under the conditions used here for MAS NMR.

4. Summary and conclusions

We have presented first 2D crystals of the green variant of proteorhodopsin. The resolution in the 2D projection map does not yet allow a statement about the PR structure but the projection map shows a ring-shaped oligomeric assembly. 2D crystals yielding low-resolution data were obtained under a wide range of conditions. This could indicate that PR is densely packed in its native membrane. Sample quality was best at basic pH and was sensitive to the choice of detergent. The combination of high CMC Triton X-100 for protein solubilisation with low CMC OG for vesicle destabilisation was found to work best. 2D crystalline PR samples were found very suitable for solid state NMR. Even aromatic side chains did cross-polarise in non-frozen samples and gave well resolved spectra. ^{15}N LG-CP spectra of selectively and uniformly labelled samples revealed both uniaxial and anisotropic protein dynamics despite packing in 2D crystals. This could have implications for structural studies: A non-frozen state is needed to obtain high spectral resolution while lower temperatures would be required to obtain non-scaled dipolar couplings for distance measurements. PR is a relatively large protein with seven transmembrane helices which may cause spectral overlap. In the absence of any 3D structure, assignment cannot be aided by structure-based chemical shift estimations such as SHIFTX [44]. Therefore, various multidimensional experiments will be needed and will benefit from methods for J-decoupling [45], fast data acquisition [46] and optimised processing schemes [47].

Acknowledgements

The help of Deryck Mills (Max Planck Institute for Biophysics) with electron microscopy and Ingrid Weber at J.W. Goethe University for technical assistance is highly appreciated. This project was financially supported by SFB 472 (Molecular Bioenergetics).

References

[1] J.M. Walter, D. Greenfield, C. Bustamante, J. Liphardt, Light-powering *Escherichia coli* with proteorhodopsin, Proc. Natl. Acad. Sci. U. S. A. 104 (2007) 2408–2412.
[2] J.L. Spudich, C.S. Yang, K.H. Jung, E.N. Spudich, Retinylidene proteins: structures and functions from archaea to humans, Annu. Rev. Cell Dev. Biol. 16 (2000) 365–392.
[3] D. Man, W. Wang, G. Sabehi, L. Aravind, A.F. Post, R. Massana, E.N. Spudich, J.L. Spudich, O. Beja, Diversification and spectral tuning in marine proteorhodopsins, EMBO J. 22 (2003) 1725–1731.
[4] O. Beja, E.N. Spudich, J.L. Spudich, M. Leclerc, E.F. DeLong, Proteorhodopsin phototrophy in the ocean, Nature 411 (2001) 786–789.
[5] G. Sabehi, R. Massana, J.P. Bielawski, M. Rosenberg, E.F. Delong, O. Beja, Novel proteorhodopsin variants from the Mediterranean and Red Seas, Environ. Microbiol. 5 (2003) 842–849.
[6] J.C. Venter, K. Remington, J.F. Heidelberg, A.L. Halpern, D. Rusch, J.A. Eisen, D. Wu, I. Paulsen, K.E. Nelson, W. Nelson, D.E. Fouts, S. Levy, A.H. Knap, M.W. Lomas, K. Nealson, O. White, J. Peterson, J. Hoffman, R. Parsons, H. Baden-Tillson, C. Pfannkoch, Y.H. Rogers, H.O. Smith, Environmental genome shotgun sequencing of the Sargasso Sea, Science 304 (2004) 66–74.
[7] O. Beja, L. Aravind, E.V. Koonin, M.T. Suzuki, A. Hadd, L.P. Nguyen, S.B. Jovanovich, C.M. Gates, R.A. Feldman, J.L. Spudich, E.N. Spudich, E.F.

DeLong, Bacterial rhodopsin: evidence for a new type of phototrophy in the sea, Science 289 (2000) 1902–1906.
[8] T. Friedrich, S. Geibel, R. Kalmbach, I. Chizhov, K. Ataka, J. Heberle, M. Engelhard, E. Bamberg, Proteorhodopsin is a light-driven proton pump with variable vectoriality, J. Mol. Biol. 321 (2002) 821–838.
[9] A.K. Dioumaev, L.S. Brown, J. Shih, E.N. Spudich, J.L. Spudich, J.K. Lanyi, Proton transfers in the photochemical reaction cycle of proteorhodopsin, Biochemistry 41 (2002) 5348–5358.
[10] L. Gomez-Consarnau, J.M. Gonzalez, M. Coll-Llado, P. Gourdon, T. Pascher, R. Neutze, C. Pedros-Alio, J. Pinhassi, Light stimulates growth of proteorhodopsin-containing marine Flavobacteria, Nature 445 (2007) 210–213.
[11] M.O. Lenz, R. Huber, B. Schmidt, P. Gilch, R. Kalmbach, M. Engelhard, J. Wachtveitl, First steps of retinal photoisomerization in proteorhodopsin, Biophys. J. 91 (2006) 255–262.
[12] G. Varo, L.S. Brown, M. Lakatos, J.K. Lanyi, Characterization of the photochemical reaction cycle of proteorhodopsin, Biophys. J. 84 (2003) 1202–1207.
[13] M. Lenz, A. Woerner, C. Glaubitz, J. Wachtveitl, Photoisomerization in proteorhodopsin mutant D97N, Photochem. Photobiol. 83 (2006) 226–231.
[14] N. Pfleger, M. Lorch, A.C. Woerner, C. Glaubitz, Characterisation of Schiff Base and Chromophore in Green Proteorhodopsin by Solid-State NMR (in press).
[15] E.S. Imasheva, K. Shimono, S.P. Balashov, J.M. Wang, U. Zadok, M. Sheves, N. Kamo, J.K. Lanyi, Formation of a long-lived photoproduct with a deprotonated Schiff base in proteorhodopsin, and its enhancement by mutation of Asp227, Biochemistry 44 (2005) 10828–10838.
[16] D. Ikeda, Y. Furutani, H. Kandori, FTIR study of the retinal Schiff base and internal water molecules of proteorhodopsin, Biochemistry 46 (2007) 5365–5373.
[17] A.J. Mason, A. Siarheyeva, W. Haase, M. Lorch, H. van Veen, C. Glaubitz, Amino acid type selective isotope labelling of the multidrug ABC transporter LmrA for solid-state NMR studies, FEBS Lett. 568 (2004) 117–121.
[18] M. Lorch, S. Fahem, C. Kaiser, I. Weber, A.J. Mason, J.U. Bowie, C. Glaubitz, How to prepare membrane proteins for solid-state NMR: a case study on the alpha-helical integral membrane protein diacylglycerol kinase from *E. coli*, ChemBioChem 6 (2005) 1693–1700.
[19] Y. Li, D.A. Berthold, H.L. Frericks, R.B. Gennis, C.M. Rienstra, Partial C-13 and N-15 chemical-shift assignments of the disulfide-bond-forming enzyme DsbB by 3D magic-angle spinning NMR spectroscopy, ChemBioChem 8 (2007) 434–442.
[20] M. Hiller, L. Krabben, K.R. Vinothkumar, F. Castellani, B.J. van Rossum, W. Kuhlbrandt, H. Oschkinat, Solid-state magic-angle spinning NMR of outer-membrane protein G from *Escherichia coli*, ChemBioChem 6 (2005) 1679–1684.
[21] D.C. Muchmore, L.P. McIntosh, C.B. Russell, D.E. Anderson, F.W. Dahlquist, Expression and nitrogen-15 labeling of proteins for proton and nitrogen-15 nuclear magnetic resonance, Methods Enzymol. 177 (1989) 44–73.
[22] R.A. Crowther, R. Henderson, J.M. Smith, MRC image processing programs, J. Struct. Biol. 116 (1996) 9–16.
[23] W.T. Franks, D.H. Zhou, B.J. Wylie, B.G. Money, D.T. Graesser, H.L. Frericks, G. Sahota, C.M. Rienstra, Magic-angle spinning solid-state NMR spectroscopy of the beta1 immunoglobulin binding domain of protein G (GB1): 15N and 13C chemical shift assignments and conformational analysis, J. Am. Chem. Soc. 127 (2005) 12291–12305.
[24] B.M. Fung, A.K. Khitrin, K. Ermolaev, An improved broadband decoupling sequence for liquid crystals and solids, J. Magn. Reson. 142 (2000) 97–101.
[25] M. Lee, W.I. Goldburg, Nuclear-magnetic-resonance line narrowing by a rotating Rf field, Physical Review 140 (1965) 1261.
[26] B.J. van Rossum, C.P. de Groot, V. Ladizhansky, S. Vega, H.J.M. de Groot, A method for measuring heteronuclear (H-1–C-13) distances in high speed MAS NMR, J. Am. Chem. Soc. 122 (2000) 3465–3472.
[27] B.J. van Rossum, H. Förster, H.J.M. de Groot, High-field and high-speed CP-MAS13C NMR heteronuclear dipolar-correlation spectroscopy of solids with frequency-switched Lee–Goldburg homonuclear decoupling, J. Magn. Reson. 124 (1997) 516–519.
[28] P.N. Unwin, R. Henderson, Molecular structure determination by electron microscopy of unstained crystalline specimens, J. Mol. Biol. 94 (1975) 425–440.
[29] A.J. Mason, G.J. Turner, C. Glaubitz, Conformational heterogeneity of transmembrane residues after the Schiff base reprotonation of bacteriorhodopsin: 15N CPMAS NMR of D85N/T170C membranes, FEBS J. 272 (2005) 2152–2164.
[30] I. Schmidt-Krey, Electron crystallography of membrane proteins: two-dimensional crystallization and screening by electron microscopy, Methods (San Diego, Calif) 41 (2007) 417–426.
[31] G.G. Prive, Detergents for the stabilization and crystallization of membrane proteins, Methods 41 (2007) 388–397.
[32] F. Millero, The thermodynamics of carbonate system in sea water, Geochim. Cosmochim. Acta (1979) 1651–1661.
[33] S. Subramaniam, T. Marti, H.G. Khorana, Protonation state of Asp (Glu)-85 regulates the purple-to-blue transition in bacteriorhodopsin mutants Arg-82-Ala and Asp-85-Glu: the blue form is inactive in proton translocation, Proc. Natl. Acad. Sci. U. S. A. 87 (1990) 1013–1017.
[34] N. Grigorieff, T.A. Ceska, K.H. Downing, J.M. Baldwin, R. Henderson, Electron-crystallographic refinement of the structure of bacteriorhodopsin, J. Mol. Biol. 259 (1996) 393–421.
[35] H. Liang, G. Whited, C. Nguyen, G.D. Stucky, The directed cooperative assembly of proteorhodopsin into 2D and 3D polarized arrays, Proc. Natl. Acad. Sci. U. S. A. 104 (2007) 8212–8217.
[36] M.R. Farrar, K.V. Lakshmi, S.O. Smith, R.S. Brown, J. Raap, J. Lugtenburg, R.G. Griffin, J. Herzfeld, Solid state NMR study of [epsilon-13C]Lys-bacteriorhodopsin: Schiff base photoisomerization, Biophys. J. 65 (1993) 310–315.
[37] J. Herzfeld, J.C. Lansing, Magnetic resonance studies of the bacteriorhodopsin pump cycle, Annu. Rev. Biophys. Biomol. Struct. 31 (2002) 73–95.
[38] H.J. de Groot, S.O. Smith, J. Courtin, E. van den Berg, C. Winkel, J. Lugtenburg, R.G. Griffin, J. Herzfeld, Solid-state 13C and 15N NMR study of the low pH forms of bacteriorhodopsin, Biochemistry 29 (1990) 6873–6883.
[39] J.G. Hu, B.Q. Sun, A.T. Petkova, R.G. Griffin, J. Herzfeld, The predischarge chromophore in bacteriorhodopsin: a 15N solid-state NMR study of the L photointermediate, Biochemistry 36 (1997) 9316–9322.
[40] K. Werner, I. Lehner, H.K. Dhiman, C. Richter, C. Glaubitz, H. Schwalbe, J. Klein-Seetharaman, H.G. Khorana, Combined solid state and solution NMR studies of alpha,epsilon-15N labeled bovine rhodopsin, J. Biomol. NMR 37 (2007) 303–312.
[41] Y. Wang, O. Jardetzky, Probability-based protein secondary structure identification using combined NMR chemical-shift data, Protein Sci. 11 (2002) 852–861.
[42] T. Mogi, T. Marti, H.G. Khorana, Structure-function studies on bacteriorhodopsin. IX. Substitutions of tryptophan residues affect protein–retinal interactions in bacteriorhodopsin, J. Biol. Chem. 264 (1989) 14197–14201.
[43] M. Hong, K. Jakes, D. Huster, Investigation of molecular motions by Lee–Goldburg cross-polarization NMR spectroscopy, J. Phys. Chem., B 106 (2002) 7355–7364.
[44] S. Neal, A.M. Nip, H. Zhang, D.S. Wishart, Rapid and accurate calculation of protein 1H, 13C and 15N chemical shifts, J. Biomol. NMR 26 (2003) 215–240.
[45] I. Scholz, S. Jehle, P. Schmieder, M. Hiller, F. Eisenmenger, H. Oschkinat, B.J. van Rossum, J-deconvolution using maximum entropy reconstruction applied to 13C–13C solid-state cross-polarization magic-angle-spinning NMR of proteins, J. Am. Chem. Soc. 129 (2007) 6682–6683.
[46] T. Szyperski, G. Wider, J.H. Bushweller, K. Wuthrich, Reduced dimensionality in triple-resonance NMR experiments, J. Am. Chem. Soc. 115 (1993) 9307–9308.
[47] C. Kaiser, J.J. Lopez, Wolfgang Bermel, C. Glaubitz, Dual Transformation Denoising for Homonuclear NMR Experiments — How to improve Spectra of Difficult Samples, Biochim. Biophys. Acta Biomem (in press).